Ab initio Based Configuration Interaction Study of the Electronic States of InP†

Biswabrata Manna, Antara Dutta, and Kalyan Kumar Das*

Physical Chemistry Section, Department of Chemistry, Jadavpur University, Calcutta 700 032, India

Received: September 16, 1999; In Final Form: December 7, 1999

Spectroscopic investigations of the low-lying electronic states of InP have been carried out by using multireference singles and doubles configuration interaction (MRDCI) method which includes relativistic effective core potentials (RECP) of the constituent atoms. There are at least 18 Λ-S states which are bound within 44 000 cm^{-1} of energy. Potential energy curves of 38 Λ-S states most of which correlate with lowest three dissociation limits have been computed. The dominant configuration of the ground state ($X^3\Sigma^-$) of the molecule is $\sigma_1^2\,\sigma_2^2\,\sigma_3^2\pi^2$ with $r_e = 2.71$ Å and $\omega_e = 248$ cm^{-1}. The ground-state dissociation energy (D_e) of InP in the absence of the spin−orbit coupling is estimated to be 1.48 eV. However, after the inclusion of the spin−orbit interaction the D_e value is reduced to 1.33 eV. All 22 Λ-S states which converge with In(^{2}P)+P(^{4}S) and In(^{2}P)+P(^{2}D) asymptotes are allowed to interact in the spin−orbit CI calculations. Effects of the spin−orbit coupling on the spectroscopic constants of lowest eight Λ-S states are studied. The zero-field splitting of the $X^3\Sigma^-$ state of InP has been estimated from the spin−orbit CI results. Several avoided crossings in the potential energy curves of Ω states are reported. Transition probabilities of many electric dipole-allowed transitions have been computed. Transitions such as $A^3\Pi-X^3\Sigma^-$, $^3\Sigma^+-^3\Pi$, $4^1\Sigma^+-2^1\Sigma^+$, and $A^3\Pi-^3\Pi$ are found to be more probable. The radiative lifetimes of six excited states, namely, $4^1\Sigma^+$, $2^3\Sigma^+$(II), $^3\Sigma^+$, $2^1\Pi$, $A^3\Pi$, and $2^1\Sigma^+$ are estimated. The $A^3\Pi$ state is short-lived with a lifetime of about 190 ns. The $A^3\Pi_{0^+}$ component survives from the predissociation. Seven allowed transitions from $A^3\Pi_{0^+}$ with $\Delta\Omega = 0$, ±1 are studied. At the lowest vibrational level ($v' = 0$), the lifetime of the $A^3\Pi_{0^+}$ component is about 456 ns.

I. Introduction

Experimental and theoretical studies on the spectroscopy of semiconductor clusters and small molecules having group III and V elements have drawn considerable attention in recent years.[1−35] These semiconductor compounds are technologically important materials because of their usefulness in the preparation of electronic devices. Among these, gallium arsenide clusters are the most widely studied compounds. In this regard one must mention the pioneering work of Smalley and co-workers[1−6] who have made several investigations on the spectroscopy and electronic structure of small clusters of these semiconducting materials. The matrix-isolated electron spin resonance (ESR) spectra of small clusters like Ge_2, Si_2, Sn_2, Ga_xAs_y, etc., have been obtained by Weltner and co-workers.[7,8] However, experimental studies on diatomic molecules of these semiconductors are seldom reported in literature. Lemire et al.[10] have studied the spectroscopy and electronic structure of the jet-cooled gallium arsenide molecule by the resonant two-photon ionization spectroscopy. Recently, small clusters of Ga and P have been characterized experimentally.[11−13] Neumark and co-workers[14−18] have applied the negative ion zero-electron kinetic photodetachment spectroscopic technique to probe the electronic states of the neutral group IV and group III−V clusters. The photodetachment spectroscopy provides information about the low-lying electronic states to which dipole-forbidden or spin-forbidden transitions may take place. Studies on In_2 P, In_2 P^-, InP_2, and InP_2^- species have been reported by Arnold and Neumark.[15] Li et al.[19] have observed infrared absorption spectra of the diatomic InX (X = P, As, Sb) molecules which are prepared by laser-vaporizing the corresponding crystals in rare gases and condensed on the gold surface at 4 K. The observed zero-field splittings [$^3\Sigma^-$ ($1X_2$)−$^3\Sigma^-$ (0^+X_1)] in the ground states of InAs and InSb have been found to be 119 and 473 cm^{-1}, respectively. However, such splitting for InP has not been reported by these authors. The vibrational progression of the low-lying $A^3\Pi$ state of InAs has been observed. The IR absorption spectrum of an argon matrix at 4 K formed by laser vaporization of the InP crystal shows two absorption bands. The sharper band at 257.9 cm^{-1} has been assigned to the diatomic InP, while the broader band at 249.3 cm^{-1} is due to In_2 P.

Balasubramanian[20,21] has made an extensive review on relativistic effects for molecules and clusters. Although much information on GaAs and InSb are known,[22−24] there seems to be very little experimental, as well as theoretical, studies of diatomic InP and InAs. The configuration interaction (CI) studies of clusters such as In_3P_2 and In_2P_3, and triatomic molecules such as In_2P, InP_2, In_2P^+, and InP_2^+ have been carried out recently by Feng and Balasubramanian.[25,26] These authors have also calculated potential energies and structural aspects of the electronic states of the isovalent gallium series.[27,28] The only ab initio CI calculations on the diatomic GaP molecule have been performed by Manna and Das.[29] The $A^3\Pi-X^3\Sigma^-$ transitions of group III−V semiconductor molecules are the subject of much discussion in recent year. Only for the gas-phase GaAs molecule, the vibronic band of the A−X system has been observed by using high-resolution spectroscopic measurement.[10] Recently, MRDCI studies of A−X bands for GaAs, GaP, and InSb molecules have been carried out.[29−31] No theoretical calculations have been attempted so far to study the electronic structure and properties of the InP molecule. The isovalent AlP molecule has been studied by Meier et al.[32] by carrying out

* Author for correspondence.

† Dedicated in memory of Dr. Gerhard Hirsch.

10.1021/jp993321+ CCC: $19.00
Published on Web 02/25/2000

large scale MRDCI calculations. Local spin density calculations for the clusters like Sb_2, Sb_4, and diatomics like CuIn, AgIn, CuGa, AgGa, etc. have been performed by Russo and co-workers.[33,34] Ab initio calculations on the electronic states of phosphides such as AsP and SbP have been performed by Toscano and Russo.[35]

In this paper, for the first time we have reported the electronic spectrum of the InP molecule. Potential energy curves and spectroscopic properties of many low-lying electronic states of InP are computed by using MRDCI method which takes care of the relativistic effects through pseudopotentials. Effects of the spin−orbit coupling on these electronic states have been studied in detail. Transition probabilities of several dipole-allowed transitions are calculated. Hence radiative lifetimes of the excited states of InP are estimated from the CI wave functions. The emphasis will be given to the $A^3\Pi \leftrightarrow X^3\Sigma^-$ transition of InP. A comparison will be made among the transition probabilities of A−X transitions of the isovalent molecules. Transitions between the Ω components with $\Delta\Omega = 0, \pm 1$ are also studied.

II. Computational Details

In recent years, ab initio based CI calculations of molecules having large number of electrons are possible due to the development of effective core potential methods which reduce the number of active electrons participating in the configuration space. In the present computation, the $4d^{10}5s^25p^1$ electrons of In and $3s^23p^3$ electrons of P are kept in the valence space, while the remaining inner electrons are replaced by the semicore type RECP of the respective atoms. The RECPs of the indium atom are taken from La John et al.,[36] while potentials of the phosphorus atom are reported by Pacios and Christiansen.[37] By using RECPs, the total number of active electrons which participate in CI is reduced to 18. The primitive Gaussian basis functions of the type (3s3p4d) of In are optimized by La John et al.[36] In the present calculations, these basis sets are augmented with one set of s and p functions of exponents 0.02 and 0.0145, respectively, taken from Balasubramanian's work.[24] The final basis set of In is, therefore, (4s4p4d) which is sufficient to polarize 5p. For the phosphorus atom, the optimized Gaussian basis sets (4s4p) of Pacios and Christiansen[37] are augmented with a set of d-polarization functions having an exponent of 0.43 a_0^{-2} from Roos and Siegbahn[38] so that the final basis set of P is (4s4p1d). These basis sets are compatible with the corresponding RECPs.

Using the above mentioned basis sets and RECPs, a self-consistent-field (SCF) calculation for the $...\pi^2\ ^3\Sigma^-$ state with 18 valence electrons is performed at each internuclear distance of InP. It generates 62 symmetry-adapted SCF-MOs which are used as one-electron functions in the CI calculations. The compositions of these SCF-MOs at all bond distances show that $4d^{10}$ electrons remain localized on the In atom. Therefore, we have kept these d-electrons frozen in the CI step. Only 8 electrons participate actively in the CI calculation. It further reduces the computational labor. We have used MRDCI codes of Buenker and co-workers[39−44] for the present calculations. In the first step, CI calculations are carried out for the Λ-S states without any spin−orbit coupling but with the inclusion of other spin-independent relativistic effects. A set of main reference configurations is chosen for each Λ-S symmetry. All singly and doubly excited configurations are generated from these reference configurations. The dimension of the total generated CI space is of the order of million. However, the size is reduced considerably by using the configuration selection procedure of Buenker and co-workers.[39,40] The dimension of the largest selected CI space with the configuration threshold of 2 μhartree becomes 32 000. The energy extrapolation technique along with the Davidson's correction[45,46] provides an estimate of the full-CI energy. The calculations have been carried out in C_{2v} subgroup. Eight roots of each irreducible representation of C_{2v} in singlet, triplet, and quintet spin multiplicities are computed separately. The sum of the squares of coefficients of the reference configurations for each root is ≥ 0.91. CI energies of each Λ−S state are plotted as a function of the internuclear distance to get the potential energy curve. For bound states, the spectroscopic parameters are estimated by fitting the potential energy curves. One-electron properties are estimated from the CI wave functions.

In the next step, the spin−orbit coupling is included in the calculation. The spin−orbit operators for In and P have been derived from the corresponding RECPs, and become available in literature.[36,37] The Λ−S CI wave functions are used as a basis for the spin−orbit calculations in the C_{2v}^2 representation. The full-CI energies estimated in the Λ−S CI calculations are kept in the diagonals of the Hamiltonian matrix, while the off-diagonal elements are computed by the RECP based spin−orbit operators and Λ−S CI wave functions. We have included all Ω components of the Λ−S eigenfunctions in the spin−orbit CI treatment. Eigenfunctions and eigenvalues obtained from the spin−orbit CI calculations provide spectroscopic features and transition properties of all low-lying Ω states of the molecule.

The fitted polynomials obtained from the potential energy curves are used to solve the numerical Schrödinger equations.[47] This will provide vibrational energies and wave functions. ^{115}In and ^{31}P isotopes are used for the calculations of vibrational frequencies of the molecule. Transition dipole moments for the pair of vibrational functions involved in a particular transition are computed. The spontaneous emission coefficients and hence transition probabilities are calculated subsequently. Radiative lifetimes of the excited states at different vibrational levels have been estimated from the respective transition probability data.

III. Results and Discussion

Spectroscopic Constants and Potential Energy Curves of Low-lying Λ-S States. The experimental atomic energy levels of both In and P atoms are known very accurately.[48] The ground state of In is of the $(5s^25p^1)\ ^2P$ symmetry, while that of phosphorus is a high-spin $(3s^23p^3)\ ^4S$ state. As the two atoms combine in their ground states, only four molecular states, namely, $^3\Sigma^-$, $^3\Pi$, $^5\Sigma^-$, and $^5\Pi$ are generated. The excited $(5s^26s^1)\ ^2S$ and $(5s^26p^1)\ ^2P$ states of In consist of Rydberg functions and are lying much above the ground state. On the other hand, the excited $(3s^23p^3)\ ^2D$ and $(3s^23p^3)\ ^2P$ states of the phosphorus atom are low-lying, and do not contain any Rydberg function. Therefore, we have focused on those electronic states which are generated from the interactions between the ground-state In and the excited-state (^2D and ^2P) P atom. There are nine singlets and nine triplets of Σ^+, $\Sigma^-(2)$, $\Pi(3)$, $\Delta(2)$, and Φ symmetries which merge with the second $In(^2P)+P(^2D)$ dissociation limit. Third dissociation limit $In(^2P)+P(^2P)$ correlates with six singlets and six triplets of $\Sigma^+(2)$, Σ^-, $\Pi(2)$, and Δ symmetries. We have computed all 34 Λ−S electronic states correlating with three lowest asymptotes. In addition, four high-lying states, namely, $^5\Sigma^+$, $2^5\Sigma^+$, $^5\Delta$, and $4^1\Sigma^+$ which dissociate into still higher limits are also studied. The computed potential energy curves of quintet and triplet Λ−S states of InP are shown in Figure 1a, while all singlet curves are plotted in Figure 1b. The transition energies (T_e), bond lengths (r_e), and vibrational

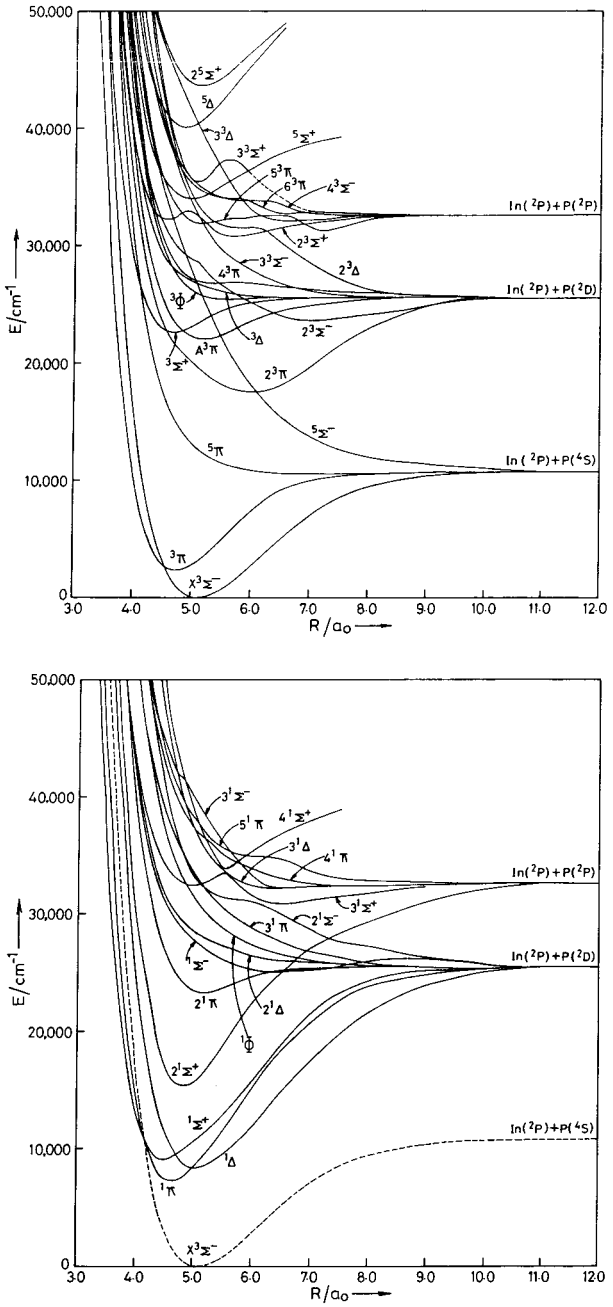

Figure 1. (a) Potential energy curves of triplet and quintet Λ−S states of InP. (b) Potential energy curves of singlet Λ−S states of InP (ground-state curve is shown by the dashed line for comparison).

TABLE 1: Spectroscopic Constants of the Low-Lying Λ−S States of InP

state	T_e/cm^{-1}	r_e/Å	ω_e/cm^{-1}
$X^3\Sigma^-$	0	2.71	248
$^3\Pi$	2 288	2.51	288
$^1\Pi$	6 953	2.46	342
$^1\Delta$	8 383	2.68	268
$^1\Sigma^+$	9 012	2.42	304
$2^1\Sigma^+$	15 471	2.56	344
$2^3\Pi$	17 574	3.17	160
$A^3\Pi$	22 082	2.75	219
$2^1\Pi$	22 431	2.74	222
$^3\Sigma^+$	22 694	2.49	256
$2^3\Sigma^-$	23 746	3.74	91
$2^3\Sigma^+$(I)	30 874	3.06	143
$3^1\Sigma^+$	31 007	3.39	142
$2^3\Sigma^+$(II)	32 292	2.40	340
$4^1\Sigma^+$	32 533	2.64	230
$^5\Sigma^+$	34 051	2.62	245
$^5\Delta$	40 175	2.56	294
$2^5\Sigma^+$	43 676	2.70	259

TABLE 2: Dominant Configurations of the Λ−S States near the Equilibrium Bond Length

state	configuration (percentage contributions)
$X^3\Sigma^-$	$\sigma_1^2\,\sigma_2^2\,\sigma_3^2\pi^2$(89)
$^3\Pi$	$\sigma_1^2\,\sigma_2^2\sigma_3\pi^3$(69),$\sigma_1^2\,\sigma_2^2\sigma_3\pi^2\pi$(14),$\sigma_1^2\,\sigma_3^2\sigma_2\pi^3$(5)
$^1\Pi$	$\sigma_1^2\,\sigma_2^2\sigma_3\pi^3$(69),$\sigma_1^2\,\sigma_2^2\sigma_3\pi^2\pi$(16)
$^1\Delta$	$\sigma_1^2\,\sigma_2^2\,\sigma_3^2\pi^2$(87)
$^1\Sigma^+$	$\sigma_1^2\,\sigma_2^2\pi^4$(39),$\sigma_1^2\,\sigma_2^2\pi^3\pi$(25),$\sigma_1^2\,\sigma_2^2\,\sigma_3^2\pi^2$(12),$\sigma_1^2\sigma_2\sigma_3\pi^4$(10)
$2^1\Sigma^+$	$\sigma_1^2\,\sigma_2^2\,\sigma_3^2\pi^2$(60),$\sigma_1^2\,\sigma_2^2\pi^3\pi$(11),$\sigma_1^2\,\sigma_2^2\pi^4$(10),$\sigma_1^2\,\sigma_2^2\,\sigma_3^2\pi\pi$(2)
$2^3\Pi$	$\sigma_1^2\,\sigma_2^2\sigma_3\pi^2\pi$(51),$\sigma_1^2\,\sigma_2^2\sigma_3\pi^3$(29)
$A^3\Pi$	$\sigma_1^2\,\sigma_2^2\sigma_3\pi^2\pi$(75),$\sigma_1^2\sigma_2\sigma_3^2\pi^2\pi$(7),$\sigma_1^2\sigma_2\sigma_3^2\pi^3$(3)
$2^1\Pi$	$\sigma_1^2\,\sigma_2^2\sigma_3\pi^2\pi$(57),$\sigma_1^2\,\sigma_2^2\sigma_3\pi\pi^2$(9),$\sigma_1^2\,\sigma_2^2\sigma_3\pi^3$(8),$\sigma_1^2\sigma_2\sigma_3^2\pi^3$(7), $\sigma_1^2\sigma_2\sigma_3^2\pi^2\pi$(7)
$^3\Sigma^+$	$\sigma_1^2\,\sigma_2^2\pi^3\pi$(66),$\sigma_1^2\,\sigma_2^2\pi^2\pi^2$(6),$\sigma_1^2\sigma_2\sigma_3\pi^3\pi$(6),$\sigma_1^2\sigma_2\sigma_3\pi^2\pi^2$(3), $\sigma_1^2\,\sigma_2^2\,\sigma_3^2\pi\pi$(3),$\sigma_1^2\sigma_2\sigma_3\pi^4$(2)
$2^3\Sigma^-$	$\sigma_1^2\,\sigma_2^2\sigma_3\sigma_4\pi^2$(42),$\sigma_1^2\,\sigma_2^2\,\sigma_3^2\pi^2$(16),$\sigma_1^2\,\sigma_2^2\sigma_3\sigma_6\pi^2$(12), $\sigma_1^2\,\sigma_2^2\sigma_3\sigma_5\pi^2$(10),$\sigma_1^2\,\sigma_2^2\pi^3\pi$(3)
$2^3\Sigma^+$	$\sigma_1^2\,\sigma_2^2\,\sigma_3^2\pi\pi$(56),$\sigma_1^2\,\sigma_2^2\pi^3\pi$(16),$\sigma_1^2\,\sigma_2^2\sigma_3\sigma_6\pi\pi$(6),$\sigma_1^2\sigma_2\sigma_3\pi^3\pi$(2), $\sigma_1^2\sigma_2\sigma_3\pi^2\pi^2$(2),$\sigma_1^2\,\sigma_2^2\pi^2\pi^2$(2)
$3^1\Sigma^+$	$\sigma_1^2\,\sigma_2^2\,\sigma_3^2\pi\pi$(60),$\sigma_1^2\,\sigma_2^2\sigma_3\sigma_6\pi\pi$(7),$\sigma_1^2\,\sigma_2^2\pi^4$(6),$\sigma_1^2\,\sigma_2^2\sigma_3^2\pi^2$(6), $\sigma_1^2\,\sigma_2^2\sigma_3\sigma_4\pi\pi$(3)
$2^3\Sigma^+$(II)	$\sigma_1^2\,\sigma_2^2\pi^3\pi$(75),$\sigma_1^2\sigma_2\sigma_3\pi^3\pi$(9)
$4^1\Sigma^+$	$\sigma_1^2\,\sigma_2^2\pi^2\pi^2$(20),$\sigma_1^2\sigma_2\sigma_3\pi^4$(18),$\sigma_1^2\,\sigma_2^2\pi^3\pi$(14), $\sigma_1^2\,\sigma_2^2\pi^4$(13), $\sigma_1^2\sigma_2\sigma_3\pi^3\pi$(9),$\sigma_1^2\sigma_2\sigma_3\pi^2\pi^2$(6),$\sigma_1^2\,\sigma_3^2\pi^4$(2)
$^5\Sigma^+$	$\sigma_1^2\sigma_2\sigma_3\pi^2\pi^2$(68),$\sigma_1^2\sigma_2^2\pi^2\pi^2$(17)
$3^3\Sigma^+$	$\sigma_1^2\sigma_2\sigma_3\pi^3\pi$(36),$\sigma_1^2\sigma_2\sigma_3\pi^2\pi^2$(23),$\sigma_1^2\,\sigma_2^2\,\sigma_3^2\pi\pi$(15),$\sigma_1^2\sigma_2^2\pi^3\pi$(12)
$^5\Delta$	$\sigma_1^2\sigma_2\sigma_3\pi^3\pi$(82),$\sigma_1^2\sigma_2\sigma_3\pi^2\pi^2$(5)
$2^5\Sigma^+$	$\sigma_1^2\,\sigma_2^2\pi^2\pi^2$(51),$\sigma_1^2\sigma_2\sigma_3\pi^3\pi$(27),$\sigma_1^2\sigma_2\sigma_3\pi^2\pi^2$(7),$\sigma_1^2\,\sigma_3^2\pi^2\pi^2$(2)

frequencies (ω_e) of 19 bound states at equilibrium are summarized in Table 1. The remaining electronic states are repulsive in nature. The ground state of InP is $X^3\Sigma^-$ which is characterized by the open shell configuration $\sigma_1^2\,\sigma_2^2\,\sigma_3^2\pi^2$. This is analogous with other isovalent semiconductor molecules like GaP, GaAs, and InSb. The equilibrium bond length and vibrational frequency of the ground state of InP are 2.71 Å and 248 cm^{-1}, respectively. No experimental or theoretical data are available for comparison. The dominant configurations of all Λ−S bound states near r_e are shown in Table 2.

Besides $X^3\Sigma^-$, the $\sigma_1^2\,\sigma_2^2\,\sigma_3^2\pi^2$ configuration generates two singlet states: $^1\Delta$ and $2^1\Sigma^+$ which are found to be strongly bound. Table 2 shows that the composition of the $2^1\Sigma^+$ state of InP requires two additional configurations: $\sigma_1^2\,\sigma_2^2\,\pi^4$ (10%) and $\sigma_1^2\,\sigma_2^2\pi^3\pi$ (11%). The calculated r_e of the $^1\Delta$ state is very much comparable with the ground-state r_e, while the In−P bond in $2^1\Sigma^+$ is about 0.15 Å shorter than the ground-state bond. Both these states have very deep potential wells with longer vibrational frequencies. The transition energy of $^1\Delta$ which is the third excited state is calculated to be 8383 cm^{-1}, while the $2^1\Sigma^+$ state is lying 15 471 cm^{-1} above the ground state. It may be noted that $X^3\Sigma^-$, $^1\Delta$, and $2^1\Sigma^+$ states originating from the same configuration dissociate into three different asymptotes in the increasing order as seen from Figure 1b.

Analogous with other isovalent molecules, the first excited state of InP is $^3\Pi$ which is generated from a single excitation $\sigma_3^2\pi^2 \rightarrow \sigma_3\pi^3$ (see Table 2). Therefore, $\sigma_1^2\,\sigma_2^2\,\sigma_3\pi^3$ is the dominant configuration of the $^3\Pi$ state. One more configuration such as $\sigma_1^2\,\sigma_2^2\,\sigma_3\pi^2\pi$ contributes significantly in describing the $^3\Pi$ state. There is a singlet counterpart which originates from the same excitation. As seen from Table 1, the $^1\Pi$ state is lying just above $^3\Pi$ with an energy gap of 4665 cm^{-1} between them.

The r_e value of the $^3\Pi$ state is 2.51 Å which is 0.2 Å shorter than the ground-state r_e. The $^1\Pi$ state has even shorter r_e and longer ω_e as compared with its triplet counterpart. The first excited $^3\Pi$ state dissociates into the lowest limit In(^{2}P)+P(^{4}S), while the $^1\Pi$ state correlates with the next higher asymptote In(^{2}P)+P(^{2}D). The greater stability of the In−P bond in $^{1,3}\Pi$ states as compared with the ground state is a general feature of these types of molecules. This is attributed to the increase in the delocalization of π molecular orbitals. The fourth excited Λ−S state of InP is a very stable $^1\Sigma^+$ state. Besides the closed shell configuration $\sigma_1^2\,\sigma_2^2\,\pi^4$ ($c^2 = 0.39$), there are three open shell configurations: $\sigma_1^2\,\sigma_2^2\,\pi^3\pi$, $\sigma_1^2\,\sigma_2^2\,\sigma_3^2\,\pi^2$, and $\sigma_1^2\sigma_2\sigma_3\pi^4$ (see Table 2) which dominate significantly in the formation of the $^1\Sigma^+$ state. The MRDCI transition energy of the $^1\Sigma^+$ state is 9012 cm^{-1}. The bond length of InP in this state is estimated to be 0.29 Å shorter than that of the ground state. The potential well of the $^1\Sigma^+$ state is also sharp with a relatively large ω_e value. There is a strong avoided crossing between the curves of $^1\Sigma^+$ and $2^1\Sigma^+$ states, and it is not very distinct from Figure 1b. However, compositions of CI wave functions of these two states show that two dominant configurations $...\pi^4$ and $...\sigma_3^2\pi^2$ interchange at bond lengths above $5.0a_0$.

Of four $^3\Pi$ states arising from $\sigma_1^2\,\sigma_2^2\,\sigma_3\pi^2\pi$, $2^3\Pi$ and $3^3\Pi$ states are found to be bound, while $4^3\Pi$ and $5^3\Pi$ are almost repulsive states. The minimum of the $2^3\Pi$ state lies 17 574 cm^{-1} above the ground state. This state has a very shallow potential well with a relatively large bond length ($r_e = 3.17$ Å) and small vibrational frequency ($\omega_e = 160$ cm^{-1}). The large r_e of the $2^3\Pi$ state makes the $2^3\Pi-X^3\Sigma^-$ transition weak. The $3^3\Pi$ state is designated as $A^3\Pi$ in analogous with the A state of GaAs for which the $A^3\Pi-X^3\Sigma^-$ band system has been experimentally observed. Therefore, the $A^3\Pi-X^3\Sigma^-$ band for InP should be observed at around 22 000 cm^{-1}. The CI estimated r_e of the $A^3\Pi$ state is 2.75 Å, while the vibrational frequency is 219 cm^{-1}. The $2^3\Pi$, $A^3\Pi$, and $4^3\Pi$ states converge to the second dissociation limit In(^{2}P)+P(^{2}D). Near r_e, there is a strong presence of the $\sigma_1^2\,\sigma_2^2\,\sigma_3\pi^3$ ($c^2 = 0.29$) in $2^3\Pi$, while the $A^3\Pi$ state is relatively pure with 75% domination of the original $\sigma_1^2\,\sigma_2^2\,\sigma_3\pi^2\pi$ configuration. The spin−orbit components of the $A^3\Pi$ state deserve special attention because of their effects on the A−X band. The repulsive $5^3\Pi$ and $6^3\Pi$ states dissociate into the third limit.

The potential energy curve of the $2^1\Pi$ state, which comes next in energy, is sharply bound with $T_e = 22\,431$ cm^{-1} and $r_e = 2.74$ Å. The composition of the $2^1\Pi$ state near r_e shows that $\sigma_1^2\,\sigma_2^2\sigma_3\pi^2\pi$ is the dominant configuration with four other configurations. There are 10 Λ−S states which originate from the $\sigma_1^2\,\sigma_2^2\sigma_3\pi^2\pi$ configuration. Of these, four states of the $^3\Pi$ symmetry namely, $2^3\Pi$, $A^3\Pi$, $4^3\Pi$, and $5^3\Pi$ are already discussed. Besides $2^1\Pi$, there are two more $^1\Pi$ states such as $3^1\Pi$ and $4^1\Pi$ which are repulsive in nature. The former state dissociates into the same limit as $2^1\Pi$, while the latter correlates with the next higher limit. The remaining three states which originate from the $\sigma_1^2\,\sigma_2^2\sigma_3\pi^2\pi$ configuration are $^1\Phi$, $^3\Phi$, and $^5\Pi$. Figure 1a and 1b show that all three states are repulsive. The $^5\Pi$ state dissociates into the lowest limit, while the two Φ states correlate with the In(^{2}P)+P(^{2}D) asymptote.

The $^3\Sigma^+$ state of InP is strongly bound with $T_e = 22\,694$ cm^{-1} lying just above the $2^1\Pi$ state. It has a shorter bond length ($r_e = 2.49$ Å). A single excitation of the type $...\pi^4 \rightarrow ...\pi^3\pi^*$ not only generates $^3\Sigma^+$ but also many other states which are mostly repulsive. From Table 2, it is evident that multiple excitations take place in the formation of the $^3\Sigma^+$ state. There is a shallow potential well in the $2^3\Sigma^-$ curve having a long equilibrium bond length ($r_e = 3.74$ Å) and small vibrational frequency ($\omega_e = 91$ cm^{-1}). An avoided crossing of the $2^3\Sigma^-$ curve with the next higher repulsive curve of the same symmetry is evident from Figure 1a. However, there is one more repulsive state ($4^3\Sigma^-$) which correlates with the In(^{2}P)+P(^{2}P) dissociation limit. The appearance of the double minima in the adiabatic potential energy curve of the $2^3\Sigma^+$ state (as seen in Figure 1a) is due to a strong avoided crossing with the curve of the higher energy $3^3\Sigma^+$ state at around $5.0a_0$. The minimum at the longer r_e is designated here as $2^3\Sigma^+$ (I) with $T_e = 30\,874$ cm^{-1}, while the more stable short-distant minimum ($r_e = 2.40$ Å) lying 32 292 cm^{-1} above the ground state is denoted as $2^3\Sigma^+$ (II) for which ω_e is found to be 340 cm^{-1}. This avoided crossing is confirmed from the composition of the CI wave functions at different bond distances. An apparent minimum near the bond length of $5.1a_0$ is noted in the adiabatic curve of the $3^3\Sigma^+$ state. The maximum at $r = 5.6a_0$ in the same curve is the result of another avoided crossing with a repulsive curve of the higher-energy $^3\Sigma^+$ state which is mainly composed of the $\sigma_1^2\,\sigma_2^2\sigma_3\sigma_4\pi^2$ configuration.

A sharp avoided crossing between the curves of $3^1\Sigma^+$ and $4^1\Sigma^+$ states is observed at $r = 5.5a_0$ as in Figure 1b. Considering the small interaction between these two states, we have designated the low-energy state as $3^1\Sigma^+$, while the high-energy state is denoted as $4^1\Sigma^+$. The $3^1\Sigma^+$ state is weakly bound with a shallow minimum at $r_e = 3.39$ Å and $\omega_e = 142$ cm^{-1}. The CI estimated transition energy of the strongly bound $4^1\Sigma^+$ state is 32 533 cm^{-1}. The diabatic curve of $4^1\Sigma^+$ is fitted for the estimation of the spectroscopic constants. The equilibrium bond length of this state is even shorter than the ground-state r_e. The diabatic $4^1\Sigma^+$ curve dissociates into the higher limit. There are at least three quintet bound states: $^5\Sigma^+$, $^5\Delta$, and $2^5\Sigma^+$ which are lying above 34 000 cm^{-1} (see Table 1) and correlate with higher asymptotes. The equilibrium bond lengths of these quintet states are shorter than that of the ground state. The $^5\Sigma^+$ state is predominantly described by a highly excited configuration $\sigma_1^2\sigma_2\sigma_3\pi^2\pi^2$. For the adequate description of these highly excited states, it may require to include Rydberg functions in the basis set.

The dissociation energy (D_e) of the ground state ($X^3\Sigma^-$) of InP is estimated to be 1.34 eV in the present calculation. This value is obtained without considering any d-correlation and spin−orbit coupling. Neither any experimental nor theoretical D_e value of InP is available to compare with our MRDCI estimated data. Earlier calculations[29] on GaP have shown a discrepancy of 0.65 eV between the calculated and observed ground-state D_e value. It also shows an improvement of 0.14 eV because of the d-electron correlation and larger basis set. We may, therefore, expect the calculated dissociation energy of InP be improved by the same amount due to the basis set extension and the correlation of 4d[10] electrons of indium in the CI step. The corrected CI-estimated D_e value of InP would become 1.48 eV. After the inclusion of the spin−orbit coupling, the calculated dissociation energy of the ground state ($X^3\Sigma^-_{0^+}$) is reduced by about 0.15 eV. Therefore, the estimated spin−orbit corrected D_e is about 1.33 eV. As a general trend, some disagreement with the experimental value is always expected because of the use of effective core potential approximations.

Spin−Orbit Coupling and Spectroscopic Parameters of Ω States. Once the spin−orbit coupling is introduced in the calculation, Λ−S states which have the same Ω components interact. The spin−orbit operators derived from RECPs are obtained from the literature.[36,37] We have included all 22 Λ−S states which dissociate into In(^{2}P)+P(^{4}S) and In(^{2}P)+P(^{2}D)

TABLE 3: Dissociation Limits of a Few Low-Lying Ω States of InP

atomic state (In + P)	molecular state	energy/cm^{-1} exptl[a]	calcd
$^2P_{1/2} + {}^4S_{3/2}$	2, 1,1,0^+,0^-	0	0
$^2P_{3/2} + {}^4S_{3/2}$	3,2,2,1,1,1,0^+,0^+0^-,0^-	2 213	2 076
$^2P_{1/2} + {}^2D_{3/2}$	2,1,1,0^+,0^-	11 362	14 728
$^2P_{1/2} + {}^2D_{5/2}$	3,2,2,1,1,0^+,0^-	11 377	14 976
$^2P_{3/2} + {}^2D_{3/2}$	3,2,2,1,1,1,0^+,0^+, 0^-,0^-	13 575	16 717
$^2P_{3/2} + {}^2D_{5/2}$	4,3,3,2,2,2,1,1,1,1,0^+,0^+, 0^-,0^-	13 590	16 965

[a] Taken from Moore's table (ref 48).

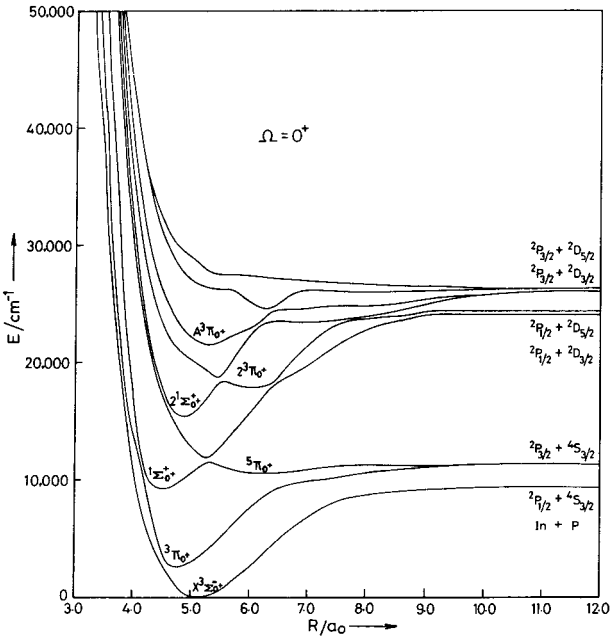

Figure 2. Potential energy curves of low-lying Ω = 0^+ states of InP.

limits for the interaction in the spin−orbit CI calculations. Table 3 shows all six asymptotes which are obtained from the spin−orbit splitting of two above mentioned dissociation limits. Relative energies of the dissociated atoms and the notations of Ω states with which these separated atoms correlate are also given in Table 3. There are 51 Ω states correlating with six asymptotes. The calculated $^2P_{3/2}-{}^2P_{1/2}$ energy splitting for In agrees very well with the observed value of 2213 cm^{-1}. The $^2D_{3/2}-{}^2D_{5/2}$ splitting of the phosphorus atom is found to be very small. The disagreement between the observed and calculated values is within the limit of accuracy of the present calculation. However, energies of four dissociation limits arising from the $^2P+{}^2D$ asymptote are higher than the experimental values by about 3300 cm^{-1}. Similar discrepancy has been also noted for GaP. This feature indicates that the ground-state dissociation energy is underestimated. Due to the lack of any experimental data, the amount of underestimation can not be confirmed.

We have plotted the potential energy curves of nine states of 0^+ symmetry in Figure 2, while another nine states with Ω = 0^- are given in Figure 3. Nine states with Ω = 1 and two states with Ω = 3 are shown in Figure 4. Potential energy curves of eleven states of Ω = 2 and one state of Ω = 4 symmetries are drawn in Figure 5. The remaining 10 repulsive curves with Ω = 1 and 3 are not plotted to avoid further complicacy in these diagrams.

Table 4 displays the spectroscopic constants and compositions of a few low-lying bound Ω states of InP. The spin−orbit components of the ground state ($X^3\Sigma^-$) of InP are separated only by 40 cm^{-1}. No experimental value of the zero-field

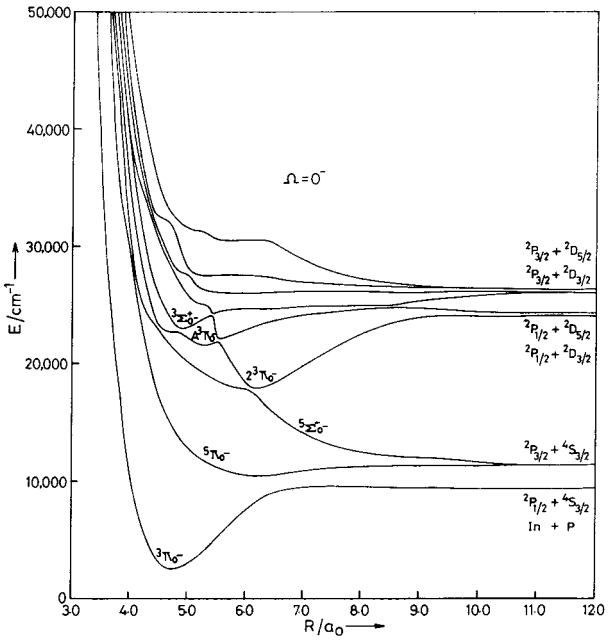

Figure 3. Potential energy curves of low-lying Ω = 0^- states of InP.

TABLE 4: Spectroscopic Constants of the Low-Lying Spin−Orbit States of InP

state	T_e/cm^{-1}	r_e/Å	ω_e/cm^{-1}	dominant states at r_e
$X^3\Sigma^-_{0^+}$	0	2.70	251	$X^3\Sigma^-$(99)[a]
$X^3\Sigma^-_1$	40	2.70	249	$X^3\Sigma^-$(99)
$^3\Pi_2$	2 113	2.51	290	$^3\Pi$(99.7)
$^3\Pi_1$	2 385	2.50	289	$^3\Pi$(95), $X^3\Sigma^-$(5)
$^3\Pi_{0^-}$	2 572	2.51	290	$^3\Pi$(99.7)
$^3\Pi_{0^+}$	2 610	2.51	289	$^3\Pi$(95), $X^3\Sigma^-$(5)
$^1\Pi_1$	7 433	2.46	327	$^1\Pi$(99)
$^1\Delta_2$	8 500	2.68	261	$^1\Delta$(99)
$^1\Sigma^+_{0^+}$	9 302	2.38	305	$^1\Sigma^+$(99)
$2^1\Sigma^+_{0^+}$	15 465	2.56	353	$2^1\Sigma^+$(99)
$2^3\Pi_2$	17 302	3.17	169	$2^3\Pi$(83), $^5\Sigma^-$(16)
$2^3\Pi_1$	17 606	3.18	161	$2^3\Pi$(84), $^5\Sigma^-$(14)
$2^3\Pi_{0^-}$	17 915	3.18	160	$2^3\Pi$(79), $^5\Sigma^-$(20)
$2^3\Pi_{0^+}$	17 925	3.19	158	$2^3\Pi$(99)
$A^3\Pi_{0^+}$	21 675	2.79	227	$A^3\Pi$(99)
$A^3\Pi_{0^-}$	21 681	2.79	217	$A^3\Pi$(99)
$A^3\Pi_1$	21 997	2.75	217	$A^3\Pi$(88), $2^1\Pi$(11)
$A^3\Pi_2$	22 656	2.70	209	$A^3\Pi$(98)

[a] Values in parentheses are percentage contributions.

splitting [$^3\Sigma^-(1X_2)-{}^3\Sigma^-(0^+X_1)$] for InP has been reported. However, for InAs and InSb, the observed splittings are 119 and 473.4 cm^{-1}, respectively. Our earlier MRDCI calculations[31] on InSb have shown a zero-field splitting of 429 cm^{-1} which agrees well with the observed value. The $X^3\Sigma^-_{0^+}$ component is found to be lower in energy than the $X^3\Sigma^-_1$ component. Both the components remain almost pure $X^3\Sigma^-$. The equlibrium bond lengths and vibrational frequencies of these two components do not change significantly. Four spin−orbit components of the first excited $^3\Pi$ state split within 500 cm^{-1} of energy. These are separated in the increasing order 2, 1, 0^-, and 0^+. As seen from Table 4, $^3\Pi_2$ and $^3\Pi_{0^-}$ components are pure $^3\Pi$ state, while $^3\Pi_1$ and $^3\Pi_{0^+}$ components have some contributions from $X^3\Sigma^-$. The transition energy of the $^1\Pi_1$ substate is increased by about 500 cm^{-1}, while other spectroscopic constants do not change much. Although $^3\Pi$ and $^1\Pi$ have the same dominant electronic configurations, there is a large energy gap (>5000 cm^{-1}) between $^3\Pi_1$ and $^1\Pi_1$ components. It prevents these two components to mix up significantly. Other singlet states such

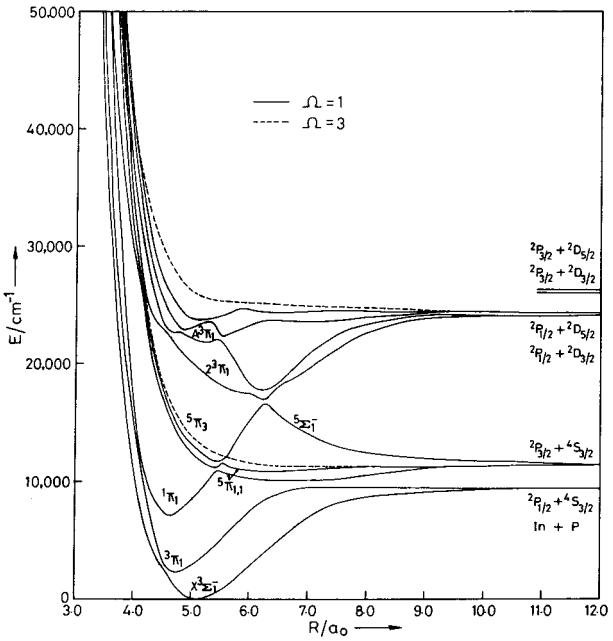

Figure 4. Potential energy curves of low-lying $\Omega = 1$ and 3 states of InP (the curve with dashed line is for $\Omega = 3$).

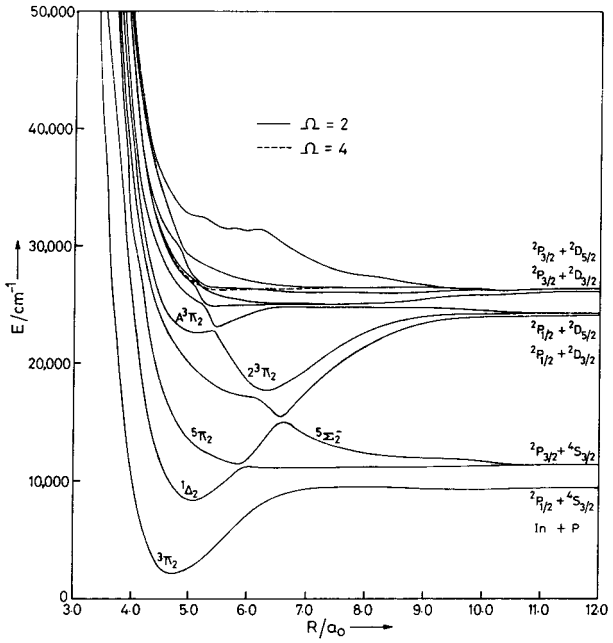

Figure 5. Potential energy curves of low-lying $\Omega = 2$ and 4 states of InP (curves with dashed lines are for $\Omega = 4$).

as $^1\Delta_2$, $^1\Sigma^+_{0^+}$, and $2^1\Sigma^+_{0^+}$ are not much affected by the spin−orbit interaction. The second $^3\Pi$ state splits into four components in the same order as the first $^3\Pi$ state. The components lie within 600 cm^{-1} energy separation and undergo several avoided crossings. The diabatic potential energy curves of $2^3\Pi_2$, $2^3\Pi_1$, $2^3\Pi_{0^-}$, and $2^3\Pi_{0^+}$ components are fitted to estimate the spectroscopic constants. Three components with $\Omega = 2$, 1, and 0^- of $^5\Sigma^-$ interact strongly with the same components of the $2^3\Pi$ state. As a result, many avoided crossings appear in the potential energy curves of these components (see Figures 3−5). The curve of the $A^3\Pi$ state, which is lying 5000 cm^{-1} above the $2^3\Pi$ state, also undergoes avoided crossings with many other curves. The spin−orbit splitting of the $A^3\Pi$ state takes place in the reverse order as compared with $^3\Pi$ and $2^3\Pi$ states. The largest energy separation between $A^3\Pi_{0^+}$ and $A^3\Pi_2$ is about 1000 cm^{-1}. Several avoided crossings make the potential energy curves of $A^3\Pi_{0^-}$ and $A^3\Pi_1$ states complicated. There is a chance of predissociation of $A^3\Pi_{0^-}$, $A^3\Pi_1$, and $A^3\Pi_2$ components mainly due to their interactions with the corresponding Ω components of the $^5\Sigma^-$ state. However, the potential well of $A^3\Pi_{0^+}$ is comparatively less interactive (see Figure 2), and hence this particular component will survive from the predissociation.

TABLE 5: Radiative Lifetimes of Some Excited Λ−S States of InP at Their Lowest Vibrational Levels

transition	partial lifetimes (μs) of the upper state $\nu' = 0$	$\nu' = 1$	$\nu' = 2$	total lifetimes (μs) of the upper state ($\nu' = 0$)
$4^1\Sigma^+ \leftrightarrow {}^1\Pi$	3.70	3.63	3.58	
$4^1\Sigma^+ \leftrightarrow 1^1\Sigma^+$	3.53	3.61	5.49	
$4^1\Sigma^+ \leftrightarrow 2^1\Sigma^+$	1.46	1.34	1.26	
$4^1\Sigma^+ \leftrightarrow 2^1\Pi$	12.16	13.03	15.82	$\tau(4^1\Sigma^+)$=0.76
$2^3\Sigma^+$(II)$\leftrightarrow {}^3\Pi$	22.85	8.67		
$2^3\Sigma^+$(II)$\leftrightarrow {}^3\Sigma^+$	7.50	11.60		$\tau(2^3\Sigma^+$(II))=5.65
$^3\Sigma^+ \leftrightarrow {}^3\Pi$	1.16	1.22	1.24	$\tau(^3\Sigma^+)$=1.16
$2^1\Pi \leftrightarrow {}^1\Delta$	3.22	3.32	3.42	
$2^1\Pi \leftrightarrow 2^1\Sigma^+$	233	222	213	$\tau(2^1\Pi)$=3.18
$A^3\Pi \leftrightarrow X^3\Sigma^-$	0.21	0.22	0.22	
$A^3\Pi \leftrightarrow {}^3\Pi$	1.71	1.55	1.49	$\tau(A^3\Pi)$=0.19
$2^1\Sigma^+ \leftrightarrow {}^1\Pi$	6.17	6.12	6.07	
$2^1\Sigma^+ \leftrightarrow 1^1\Sigma^+$	12.23	12.15	12.04	$\tau(2^1\Sigma^+)$=4.10

Transition Moments and Radiative Lifetimes. The only experimental study on InP known so far, is the infrared absorption spectroscopy of the molecule in argon-gas matrix at 4 K. No theoretical data for transition probabilities of any electronic transition are available in literature. However, many dipole-allowed transitions can be predicted from the present MRDCI study. Transition probabilities of these transitions are estimated from the transition dipole moment data. Subsequently, the partial radiative lifetimes of some upper states of InP at three lowest vibrational levels are reported in Table 5. Transitions from $4^1\Sigma^+$, $2^3\Sigma^+$(II), $^3\Sigma^+$, $2^1\Pi$, $A^3\Pi$, $2^3\Pi$, and $2^1\Sigma^+$ states to all possible lower states are considered here. However, some of these transitions are very weak. Transition moments as well as energy differences involving the $2^3\Pi-X^3\Sigma^-$ transition are sufficiently large, but the Franck−Condon overlap factors are very small. As a result, the $2^3\Pi-X^3\Sigma^-$ transition is considerably weak. Another possible transition such as $2^3\Pi-{}^3\Pi$ is also not so strong enough to be observed experimentally. For this transition, the Franck−Condon overlap term is negligibly small due to much longer r_e of the upper state as compared with r_e of the lower state. Transition probabilities of two transitions, namely, $2^1\Pi-{}^1\Pi$ and $2^1\Pi-{}^1\Sigma^+$, are also very small due to the shifted equlibrium bond length of the $2^1\Pi$ state.

The $4^1\Sigma^+$ state undergoes four symmetry-allowed transitions: $4^1\Sigma^+-{}^1\Pi$, $4^1\Sigma^+-{}^1\Sigma^+$, $4^1\Sigma^+-2^1\Sigma^+$, and $4^1\Sigma^+-2^1\Pi$. Of these, $4^1\Sigma^+-2^1\Sigma^+$ is found to be the strongest transition, while the $4^1\Sigma^+-2^1\Pi$ transition is much weaker because of the small energy difference. The $4^1\Sigma^+-2^1\Sigma^+$ transition-moments are significantly large, but the overlap between the diabatic potential curves of these two states is somewhat small. The estimated total radiative lifetime of the $4^1\Sigma^+$ state at $\nu' = 0$ is found to be 0.76 μs.

Transitions from the $2^3\Sigma^+$(I) state having a longer r_e are found to be weak. We have calculated transition probabilities of transitions from the $2^3\Sigma^+$(II) state which has a shorter r_e. At the lowest vibrational level ($\nu' = 0$), the $2^3\Sigma^+$(II)$-{}^3\Sigma^+$ transition is found to be three times stronger than the $2^3\Sigma^+$(II)$-{}^3\Pi$ transition. Adding transition probabilities, the total lifetime of $2^3\Sigma^+$(II) at $\nu' = 0$ is calculated to be about 5.65 μs. There is only one transition allowed from the $^3\Sigma^+$ state. Our calculations

TABLE 6: Radiative Lifetimes of the $A^3\Pi_{0^+}$ State of InP at $\nu' = 0$

transition	lifetimes of the $A^3\Pi_{0^+}$ state (μs)
$X^3\Sigma^-_{0^+} \leftrightarrow A^3\Pi_{0^+}$	73.3
$^3\Pi_{0^+} \leftrightarrow A^3\Pi_{0^+}$	770.0
$2^1\Sigma^+_{0^+} \leftrightarrow A^3\Pi_{0^+}$	3.3×10^3
$^1\Sigma^+_{0^+} \leftrightarrow A^3\Pi_{0^+}$	1.1×10^9
$X^3\Sigma^-_1 \leftrightarrow A^3\Pi_{0^+}$	0.46
$^3\Pi_1 \leftrightarrow A^3\Pi_{0^+}$	4.7×10^4
$^1\Pi_1 \leftrightarrow A^3\Pi_{0^+}$	42.4×10^6
total lifetimes $\tau(A^3\Pi_{0^+})$	0.456

predict that a reasonably strong $^3\Sigma^+ - ^3\Pi$ transition should be observed at around 20 400 cm^{-1}. The estimated radiative lifetime of the $^3\Sigma^+$ state is 1.16 μs. Four transitions involving the $2^1\Pi$ state are allowed. These are $2^1\Pi - ^1\Pi$, $2^1\Pi - ^1\Sigma^+$, $2^1\Pi - ^1\Delta$, and $2^1\Pi - 2^1\Sigma^+$ of which first two transitions are extremely weak due to small Franck–Condon overlap terms. The $2^1\Pi - ^1\Delta$ transition is sufficiently strong, while $2^1\Pi - 2^1\Sigma^+$ has smaller transition probabilities. As seen from Table 5, partial lifetimes of the $2^1\Pi$ state in the $2^1\Pi - ^1\Delta$ band is just above 3 μs, while for the $2^1\Pi - 2^1\Sigma^+$ band, it is around 200 μs. Total lifetime of $2^1\Pi$ at $\nu' = 0$ is, therefore, estimated to be 3.18 μs.

The strongest transition which should be observed in InP at 22 000 cm^{-1} is due to $A^3\Pi - X^3\Sigma^-$. The partial lifetimes of $A^3\Pi$ at low-lying vibrational levels are around 200 ns. The vibronic bands of the A–X system have been observed for the gas-phase isovalent GaAs molecule by using high-resolution spectrometric studies. However, similar experimental studies for InP have not been attempted. The second allowed transition $A^3\Pi - ^3\Pi$ is much weaker with smaller transition dipole moments. Combining transition probabilities of these two transitions, the estimated radiative lifetime of the $A^3\Pi$ state is 190 ns. Two more transitions such as $2^1\Sigma^+ - ^1\Pi$ and $2^1\Sigma^+ - ^1\Sigma^+$ are reported in Table 5. The former transition is found to be stronger than the latter.

Since the $A^3\Pi_{0^+}$ component does not undergo predissociation, we have studied probable transitions from this particular component. Table 6 shows partial lifetimes of $A^3\Pi_{0^-}$ at the lowest vibrational level ($\nu' = 0$) involving seven transitions. The strongest transition has been found to be $X^3\Sigma^-_1 - A^3\Pi_{0^+}$. However, the $X^3\Sigma^-_{0^+} - A^3\Pi_{0^+}$ transition is reasonably strong, while all other transitions are weak. The MRDCI estimated total lifetime of the $A^3\Pi_{0^+}$ state is 456 ns.

Comparison with the Isovalent AlP and GaP Molecules. Spectroscopic properties of InP obtained from the present calculations may be compared with those of the isovalent AlP and GaP molecules.[29,32] All three molecules have identical ground states of the $X^3\Sigma^-$ symmetry. Due to the larger size of the indium atom, the In–P bond in the ground state is longer than both Al–P and Ga–P bonds. The first excited $^3\Pi$ state of InP is described by the same configuration $...\sigma_3\pi^3$ as in other two molecules. The bond lengths of the $^3\Pi$ state for all three molecules are noticeably short. This is because of the greater stability of the σ_3 MO than π as a general rule for these molecules.[49] The computed $^3\Pi - X^3\Sigma^-$ energy separation of AlP, GaP, and InP are 645, 782, and 2288 cm^{-1}, respectively, as per expectation. The $^1\Sigma^+$ and $2^1\Sigma^+$ states of all three molecules interact similarly resulting an avoided crossing at around $r = 5.0a_o$ in their potential energy curves. Although the interaction between $3^1\Sigma^+$ and $4^1\Sigma^+$ is not noted in the potential energy curves of AlP,[32] sharp avoided crossings between these two curves in both GaP and InP are prominant. The energy gap between $2^1\Sigma^+$ and $3^1\Sigma^+$ states is sufficiently large to have any mixing. Both GaP and InP molecules have a strongly bound $4^1\Sigma^+$ state in the region of 32000–35000 cm^{-1}, while for AlP, this state has not been calculated so far.

A strong avoided crossing between the potential energy curves of $2^3\Pi$ and $A^3\Pi$ of AlP has been noted at the bond length above $5.0a_o$, while for GaP and InP, the interactions between these two curves are weak. A shoulder appears in the potential energy curve of the $2^3\Pi$ state at the bond length below $5.0a_o$. A double minima has been reported in the potential energy curve of the $2^3\Pi$ state of AlP. The potential energy curves of $2^3\Pi$ for AlP, GaP, and InP look alike with a shallow well at the longer bond distance. The nature of the curve of the third $3^3\Pi$ state, which is designated as A, is somewhat different for AlP as compared with that of GaP or InP. The $A^3\Pi - X^3\Sigma^-$ transitions of all three molecules are important from the experimental point of view. Although no experimental results are available for either of these molecules, MRDCI calculations on GaP and InP show that the reasonably strong A–X transitions should take place at around 24 000 and 22 000 cm^{-1}, respectively. For AlP, such transition is expected to be observed near 21 800 cm^{-1}. The calculated radiative lifetimes of $A^3\Pi$ for GaP and InP are 140 and 190 ns, respectively, while for AlP, this is not known as yet.

One may note that the repulsive curves of the $^5\Sigma^-$ symmetry for these molecules cross the curves of $2^3\Pi$ and $A^3\Pi$ state in a similar way. Hence, 0^-, 1, and 2 components which are common in $^5\Sigma^-$ and $^3\Pi$, interact strongly which results in their predissociations, while the remaining component $^3\Pi_{0^+}$ survives. As a result, the $A^3\Pi_{0^+} - X^3\Sigma^-_{0^+}$ transition should be observed for all these molecules. Such predissociations are observed only for GaAs which is however isovalent with the phosphides considered here.

IV. Concluding Remarks

Ab initio based MRDCI studies using RECPs and its compatible Gaussian basis sets show that the ground-state symmetry of the InP molecule is $X^3\Sigma^-$ similar with isovalent semiconductor molecules of group III and V such as AlP, GaP, GaAs, InSb, etc. The present calculations reveal that there are at least 18 bound $\Lambda - S$ states within 44 000 cm^{-1} of energy. The electronic spectra of InP look very similar with that of the GaP molecule. None of the electronic states of InP has been studied before. The equilibrium bond length and vibrational frequency of the ground state of InP are 2.71 Å and 248 cm^{-1}, respectively. As noted previously, the use of RECPs generally overestimates r_e and underestimates ω_e. We expect the observed r_e would be shorter and ω_e would be larger to some extent. Three high-lying quintet states such as $^5\Sigma^+$, $^5\Delta$, and $2^5\Sigma^+$ are found to be strongly bound, while two low-lying high-spin states, $^5\Pi$ and $^5\Sigma^-$, are repulsive. The MRDCI estimated ground-state dissociation energy of InP is about 1.48 eV. No experimental value is available for comparison. However, some discrepancy will always be expected because of the effective core potential approximations. Extensive spin–orbit calculations have been carried out by interacting all 22 $\Lambda - S$ states which correlate with the lowest two dissociation limits. The zero-field splitting $[^3\Sigma^-(1X_2) - ^3\Sigma^-(0^+X_1)]$ in the ground state of InP is predicted to be 40 cm^{-1} only. The observed zero-field splittings[19] for InAs and InSb are 119 and 473.4 cm^{-1}, respectively. However, for InP, the expected value should be less than 100 cm^{-1}, and it agrees with our calculated value. The present calculations suggest that the $X^3\Sigma^-_{0^+}$ component is lower than $X^3\Sigma^-_1$. In general, effects of the spin–orbit coupling are not significantly large. Potential energy curves of the Ω-components of $A^3\Pi$ reveal predissociations of three components such as

$A^3\Pi_{0^-}$, $A^3\Pi_1$, and $A^3\Pi_2$ due to their interactions with the similar components of the repulsive $^5\Sigma^-$ state. The remaining component ($A^3\Pi_{0^+}$) survives from the predissociation.

The strongest transition which should be observed at around 22 000 cm^{-1} is $A^3\Pi-X^3\Sigma^-$. Besides this, transitions such as $A^3\Pi-{}^3\Pi$ and $^3\Sigma^+-{}^3\Pi$ are reasonably strong. The total lifetime of the $A^3\Pi$ state at the lowest vibrational level ($\nu' = 0$) is about 190 ns. In presence of the spin−orbit coupling, the $X^3\Sigma_1^- - A^3\Pi_{0^+}$ transition is the strongest, and the total radiative lifetime of the $A^3\Pi_{0^+}$ component at $\nu' = 0$ is 456 ns.

Acknowledgment. The authors thank Professor R. J. Buenker, Wuppertal, Germany, for giving the permission to use his MRDCI program packages. The financial support from the CSIR, Government of India, under Grant 01(1427)/96/EMR-II is gratefully acknowledged.

References and Notes

(1) O'Brien, S. C.; Liu, Y.; Zhang, Q.; Heath, J. R.; Tittel, F. K.; Curl, R. F.; Smalley, R. E. *J. Chem. Phys.* **1986**, *84*, 4074.
(2) Liu, Y.; Zhang, Q.; Tittel, F. K.; Curl, R. F.; Smalley, R. E. *J. Chem. Phys.* **1986**, *85*, 7434.
(3) Zhang, Q.; Liu, Y.; Curl, R. F.; Tittel, F. K.; Smalley, R. E. *J. Chem. Phys.* **1988**, *88*, 1670.
(4) Jin, C.; Taylor, K.; Conciecao, J.; Smalley, R. E. *Chem. Phys. Lett.* **1990**, *175*, 17.
(5) Wang, L.; Chibante, L. P. F.; Tittel, F. K.; Curl, R. F.; Smalley, R. E. *Chem. Phys. Lett.* **1990**, *172*, 335.
(6) Lou, L.; Wang, L.; Chibante, L. P. F.; Laaksonen, R. T.; Nordlanden, P.; Smalley, R. E. *J. Chem. Phys.* **1991**, *94*, 8015.
(7) Van Zee, R. J.; Li, S.; Weltner, W., Jr. *J. Chem. Phys.* **1993**, *98*, 4335.
(8) Li, S.; Van Zee, R. J.; Weltner, W., Jr. *J. Chem. Phys.* **1994**, *100*, 7079.
(9) Knight, L. B., Jr.; Petty, J. T. *J. Chem. Phys.* **1988**, *88*, 481.
(10) Lemire, G. W.; Bishea, G. A.; Heidecke, S. A.; Morse, M. D. *J. Chem. Phys.* **1990**, *92*, 121.
(11) Cowley, A. H.; Jones, R. A. *Angew. Chem., Int. Ed. Engl.* **1989**, *102*, 1235.
(12) Cowley, A. H.; Jones, R. A. *Angew. Chem., Int. Ed. Engl.* **1989**, *28*, 1208.
(13) Niediek, K.; Neumullar, B. *Chem. Ber.* **1994**, *127*, 67.
(14) Xu, C.; deBeer, E.; Arnold, D. W.; Arnold, C. C.; Neumark, D. M. *J. Chem. Phys.* **1994**, *101*, 5406.
(15) Arnold, C. C.; Neumark, D. M. *Can. J. Phys.* **1994**, *72*, 1322.
(16) Arnold, C. C.; Neumark, D. M. *J. Chem. Phys.* **1994**, *100*, 1797.
(17) Arnold, C. C.; Neumark, D. M. *J. Chem. Phys.* **1994**, *99*, 3353.
(18) Burton, G. R.; Xu, C.; Arnold, C. C.; Neumark, D. M. *J. Chem. Phys.* **1996**, *104*, 2757.
(19) Li, S.; Van Zee, R. J.; Weltner, W., Jr. *J. Phys. Chem.* **1994**, *98*, 2275.
(20) Balasubramanian, K. *Relativistic Effects in Chemistry Part A. Theory and Techniques*; Wiley Intersciences: New York, 1997.
(21) Balasubramanian, K. *Relativistic Effects in Chemistry Part B. Applications to Molecules and Clusters*; Wiley Intersciences: New York, 1997.
(22) Balasubramanian, K. *J. Mol. Spectrosc.* **1990**, *139*, 405.
(23) Meier, U.; Peyerimhoff, S. D.; Bruna, P. J.; Grein, F. *J. Mol. Spectrosc.* **1989**, *134*, 259.
(24) Balasubramanian, K. *J. Chem. Phys.* **1990**, *93*, 507.
(25) Feng, P. Y.; Balasubramanian, K. *Chem. Phys. Lett.* **1998**, *283*, 167.
(26) Feng, P. Y.; Balasubramanian, K. *Chem. Phys. Lett.* **1998**, *284*, 313.
(27) Feng, P. Y.; Balasubramanian, K. *Chem. Phys. Lett.* **1997**, *265*, 41.
(28) Feng, P. Y.; Balasubramanian, K. *Chem. Phys. Lett.* **1997**, *265*, 547.
(29) Manna, B.; Das, K. K. *J. Mol. Struct. (Theochem)* **1999**, *467*, 135.
(30) Manna, B.; Das, K. K. *J. Phys. Chem.* **1998**, *A102*, 9876.
(31) Manna, B.; Dutta, A.; Das, K. K. *J. Mol. Struct. (Theochem)* **1999**. In press.
(32) Meier, U.; Peyerimhoff, S. D.; Bruna, P. J.; Karna, S. P.; Grein, F. *Chem. Phys.* **1989**, *130*, 31.
(33) Musolino, V.; Toscano, M.; Russo, N. *J. Comput. Chem.* **1990**, *11*, 924.
(34) Oranges, T.; Musolino, V.; Toscano, M.; Russo, N. *Z. Phys. D* **1990**, *17*, 133.
(35) Toscano, M.; Russo, N. *Z. Phys. D* **1992**, *22*, 683.
(36) LaJohn, L. A.; Christiansen, P. A.; Ross, R. B.; Atashroo, T.; Ermler, W. C. *J. Chem. Phys.* **1987**, *87*, 2812.
(37) Pacios, L. F.; Christiansen, P. A. *J. Chem. Phys.* **1985** *82*, 2664.
(38) Roos, B.; Siegbahn, P. *Theor. Chim. Acta* **1970**, *17*, 199.
(39) Buenker, R. J.; Peyerimhoff, S. D. *Theor. Chim. Acta* **1974**, *35*, 33.
(40) Buenker, R. J.; Peyerimhoff, S. D. *Theor. Chim. Acta* **1975**, *39*, 217.
(41) Buenker, R. J. *Int. J. Quantum Chem.* **1986**, *29*, 435.
(42) Buenker, R. J.; Peyerimhoff, S. D.; Butcher, W. *Mol. Phys.* **1978**, *35*, 771.
(43) Buenker, R. J.; In *Proceedings of the Workshop on Quantum Chemistry and Molecular Physics*; Burton, P., Ed.; University Wollongong: Wollongong, Australia, 1980. *Studies in Physical and Theoretical Chemistry*; Carbó, R., Ed.; Elsevier: Amsterdam, 1981; Vol. 21 (Current Aspects of Quantum Chemistry).
(44) Buenker, R. J.; Phillips, R. A. *J. Mol. Struct. (Theochem)* **1985**, *123*, 291.
(45) Davidson, E. R. In *The World of Quantum Chemistry*; Daudel, R., Pullman, B., Ed.; Reidel: Dordrecht, 1974.
(46) Hirsch, G.; Bruna, P. J.; Peyerimhoff, S. D.; Buenker, R. J. *Chem. Phys. Lett.* **1977**, *52*, 442.
(47) Cooley, J. W. *Math. Comput.* **1961**, *15*, 363.
(48) Moore, C. E. *Atomic Energy Levels*; National Bureau of Standards: Washington, DC; 1971; Vol 3.
(49) Bruna, P. J.; Peyerimhoff, S. D. In *Advances in Chemical Physics*; Lawley, K. P., Ed.; Wiley: New York, 1987; Vol. 67, p 1.